Original Contribution

Comparison of a Capacitive and a Cavity Slot Radiative Applicator for Regional Hyperthermia

HUGO KROEZE[1]*, MASAKI KOKUBO[2], JEROEN B. VAN DE KAMER[1],
ASTRID A.C. DE LEEUW[1], MAKOTO KIKUCHI[3],
MASAHIRO HIRAOKA[4] AND JAN J.W.LAGENDIJK[1]

[1]Department of Radiotherapy, University Medical Centre Utrecht, Utrecht, The Netherlands.
[2]Institute of Biomedical Research and Innovation, Chuo, Kobe, Japan.
[3]Department of Medical Engineering, National Defence Medical College, Tokorozawa, Saitama, Japan.
[4]Department of Therapeutic Radiology and Oncology, Kyoto University Graduate School of Medicine, Kyoto, Japan.

Abstract : The performance of a capacitive and a radiative annular phased array applicator for regional hyperthermia is compared in a model study, for an agar-bone phantom and a structured patient anatomy with a prostate tumour. The capacitive applicator is a model of the Thermotron RF8 device, operating at 8 MHz. Its performance is improved by the use of very cold overlay boli with a suitable salinity. The radiative applicator is a three ring, cavity slot annular array applicator, operating at 150 MHz. The Specific Absorption Rate (SAR) distribution in the cavity slot applicator is optimized by phase-amplitude control. Comparison of both SAR and thermal distributions shows that the radiative applicator can generate good tumour heating in the pelvic region and avoid the overheating of superficial fat layers and muscle tissue seen in the capacitive applicator.

Key Words : regional hyperthermia, capacitive heating, radiative heating, optimization.

Introduction

The Thermotron RF8 system (Yamamoto VINITA Co., Osaka, Japan) is widely in use in Asian countries for the hyperthermia treatment of tumours. The RF8 system is a capacitive heating device operating at 8 MHz, where the patient is placed between two electrodes which are connected to a high power RF generator [1] [2]. The patient is coupled to the electrodes with bolus bags, containing saline water of low temperature. The positive effect of capacitive regional hyperthermia was demonstrated in a randomized study of radiation therapy versus thermoradiotherapy in stage IIIB cervical carcinoma [3]. The basic characteristics of capacitive hyperthermia are related to the $\vec{E}$-field orientation perpendicular to the body surface and the low RF frequency [4]. These properties result in absorbed power distributions highly governed by tissue anatomy [4]. Characteristics are overheating of subcutaneous fat, edge effects

and insufficient penetration depth [5]. These effects can be partially overcome by intensive surface cooling to avoid overheating of fat [6], the use of water pads (i. e. overlay bolus sheets) larger than the electrodes to reduce edge effects [7-9], and/or increasing the size of the electrodes to improve penetration depth [1] [2].

Clinical studies show a good performance of capacitive heating techniques in the head and neck region and the thorax, fair results in the upper abdomen and moderate results in the lower abdomen and pelvis [5] [10].

Parallel to the advent of capacitive applicator systems, several radiative annular array systems have been developed : the early BSD Annular Array (AA) system [11], the BSD-2000 SIGMA 60 applicator [12], the Amsterdam 4 Waveguide system [13] and the Utrecht Coaxial TEM system [14], operating in the range from 70 MHz to 110 MHz. These systems are characterized by an $\vec{E}$-field oriented parallel to the cranial-caudal axis of the patient. A randomized trial by Van der Zee et al. [15] established the positive effect of regional hyperthermia with radiative applicators, combined with external radiotherapy on pelvic tumours. These early radiative systems are characterized by a deep interference maximum of the absorbed power distribution, but also by treatment limiting local hot spots [16] [17], systemic stress [18] and general discomfort [19].

Egawa et al. [20] compared the performance of the Thermotron RF-8 system with the Annular Array (AA) system [11] in a study with 13 patients with abdominal and pelvic tumours. The study concluded that both systems have advantages and disadvantages, and did not indicate either of the applicators as superior. To resolve these disadvantages, both capacitive and radiative hyperthermia systems became subject of further development and technical improvement.

Recently, hyperthermia treatment planning (HTP) systems have been developed for radiative applicator systems [21-26]. It has been shown using these HTP's that a new generation of radiative systems can be developed using multiple antenna rings, phase amplitude control and a higher RF frequency [23] [24] [27] [28].

The characteristics of a new radiative cavity slot antenna have been described by Kroeze et al. [28]. Using a quasi static model Kroeze et al. [4] developed a HTP system for capacitive regional hyperthermia.

Using both HTP systems, the current paper compares the performance of the RF8 capacitive system with the new design of the cavity slot radiative hyperthermia applicator, using a Japanese patient anatomy with a prostate tumour. The basic performance of both applicator types is investigated in a patient shaped agar-bone phantom, showing the influence of the bone structure on the SAR distribution in the capacitive applicator. The cavity slot radiative applicator is still under study, a prototype has yet to be build. This paper is hence limited to a simulation study.

Methods

Patient model and agar bone phantom

The patient model, Fig. 1, has been derived from a 40cm CT data set (slice thickness 5mm) of a male, Asian patient with a prostate tumour. All slices in Fig. 1 are displayed centrally through the tumour. The CT data set was segmented by Hounsfield Unit thresholding [29] and down-scaled to 5mm³ resolution, using the 'winner take all' algorithm [30]. This method results in a patient model with regions that are

assigned homogeneous dielectric properties. The tumour was manually outlined by a physician.

The SAR distribution in a patient in a capacitive heating device depends largely on the distribution of fat and bone [4]. To separate the effects of bone and fat in the comparison of a capacitive and a radiative applicator, the comparison is first made in the patient shaped agar-bone phantom. The agar-bone phantom is created by assigning fat, muscle and tumour tissue the dielectric properties equivalent to saline water with 0.22% NaCl at 25°C [31]. These values are equal to those used by Tomimatsu *et al.* [8] [9] in a phantom study.

The dielectric properties used in the SAR computations are listed in Table I. The values for tissue have been derived from literature [32-34], those of the saline water in the bolus bags from Kato *el al.* [7].
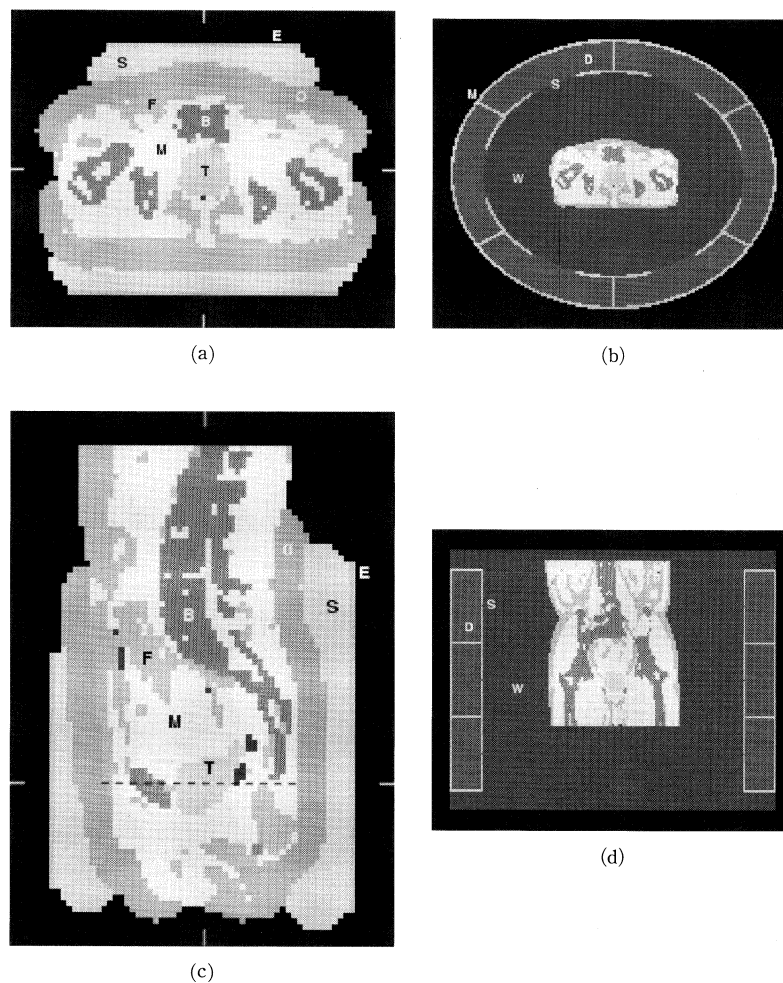

(a)

(b)

(c)

(d)

Fig. 1: Patient model (a, c) in RF8 applicator and (b, d) in cavity slot applicator. The CT data set is segmented in muscle (M), fat (F), bone (B) and tumour (T) tissue, (a, b) transversal, (c) sagittal and (d) coronal slice centrally through the tumour. The RF8 applicator is modeled with circular electrodes (E) coupled to the patient with saline bolus bags (S) and overlay boli (O). The cavity slot applicator (b, d) is constructed from metal sheets (M), farming cavities filled with deionised water (D) with radiating slots (S). The space between the applicator and the patient is filled with tapwater (W).

Table I: Dielectric properties of applicator materials and patient tissues at 8 MHz and 150 MHz.

frequency material/tissue	8MHz ε_r	$\sigma(Sm^{-1})$	150MHz ε_r	$\sigma(Sm^{-1})$
bolus water	73.5	3.0	—	—
overlay bol.	78.6	0.45	—	—
tap water	—	—	76.5	0.042
deionised water	—	—	76.5	0.001
air	1.0	0	1.0	0
muscle	160	0.64	75.0	0.75
fat	29.6	0.053	10.0	0.06
bone	36.8	0.043	10.0	0.05
tumour	160	0.64	65.0	0.74
agar	77.6	0.39	77.6	0.39

RF8 SAR model

The SAR distributions in the patient model have been computed using the quasistatic treatment planning system for capacitive hyperthermia [4]. The validity of the quasistatic approximation for capacitive HTP has been validated by comparison with an analytic solution. The patient was treated in a Thermotron RF8 applicator with an anterior electrode of 21cm and a posterior electrode of 30cm. In order to optimize the heating conditions in the RF8 applicator, overlay boli [7-9] were incorporated in the patient simulation. The model of the overlay boli was created by growing an anterior and posterior 'blanket' with a thickness of 25mm on the patient model, and positioning the normal electrode bolus bags against them (Fig. 1 (a) and 1 (c)). The salinity of the electrode bolus bags and overlay boli were taken from a phantom study by Kato *et al.* [7] as the values that result in the best ratio of central SAR with respect to SAR in the superficial fat. As the main function of the overlay boli is the suppression of high SAR values in the superficial fat, they have not been employed in the simulation with the agar-bone phantom.

The definition of the applicator electrodes with bolus bags is done using the Generic Object Format [35]. The metal electrode plates are set at a fixed potential of 1V, respectively-1V, with a frequency of 8 MHz. The QUASAR computation of the power density distribution takes about 40 minutes with a standard PC (800 MHz) and requires about 7.5 MB RAM. From the power density distribution a SAR distribution is derived.

Cavity slot applicator SAR model

The cavity slot applicator consists of three elliptical rings of six cavity slot antennas each [28]. The patient and the antenna array are submerged in a volume of tapwater, in order to couple the patient to the antennas. The operating frequency of the cavity slot applicator is chosen to be 150 MHz; this frequency was found to be optimal for the effective heating of deep situated tumours and good hot spot avoiding ability in normal tissue [27] [28]. The cavities are filled with deionised water in order to reduce the dimensions of the antenna array. The length of the slots and the depth of the cavities are approximately $\lambda_{water}/2$ and $\lambda_{water}/4$ respectively, in order to obtain a resonant antenna at the operating frequency. The Finite Difference Time Domain (FDTD)-core of our Regional Hyperthermia Treatment Planning (HTP) system [25] was used to compute $\vec{E}$-field distributions in the patient model.

The number of iterations was 12000; convergence was tested by observing the time evolution of $|\vec{E}|$

at a test point in the patient and found to be stable within 0.1% of the end value. The $\vec{E}$-field distribution is computed for each separate slot antenna.

The active slot is excited with a source, generating a triple cosine pulse of unit amplitude, placed in the gap in the metal sheet halfway along the length of the slot. The source has an impedance of 50Ω, implemented as described by Piket-May *et al.*[36]. The inactive slots are terminated with the same impedance in order to achieve correct simulation of coupling effects between the antennas.

A typical $\vec{E}$-field computation requires about 200 MB RAM and takes about six hour on a 800 MHz standard personal computer. The SAR distribution for N $\vec{E}$-fields is computed according to equation (1) using a steering vector **V**, where $\mathbf{V}_i$ is the complex number representing the amplitude and phase of each antenna[37].

$$\mathrm{SAR}(\vec{r}) = \frac{\sigma(\vec{r})}{2\rho(\vec{r})} \left| \sum_i^N \vec{E}(\vec{r})_i \mathbf{V}_i \right|^2 \tag{1}$$

In equation (1) SAR $(\vec{r})$ is the SAR, $\vec{E}(\vec{r})$ i is the $\vec{E}$-field for antenna i, $\sigma(\vec{r})$ and $\rho(\vec{r})$ are respectively the conductivity and density of the voxel at $\vec{r}$.

SAR optimization

The SAR distribution in the RF8 applicator is optimized with the application of overlay boli and selection of the optimal salinity of both bolus elements (see RF8 SAR model).

The SAR distribution in the cavity slot applicator is optimized by maximizing the objective function defined as the ratio of total SAR in the tumour versus total SAR in muscle and fat (or in agar in the agar-bone phantom). An optimizer routine modifies the steering vector **V** in small steps from a start vector in the direction of maximal improvement of the SAR ratio[28]. The optimizer constrains the power per antenna to 10% of the total power in order to avoid an unrealistic power distribution at the antennas. In order to avoid high SAR values in certain subvolumes, these subvolumes can be assigned a weight factor to reduce the local SAR value. In this study a three step optimization technique was employed. In the first step the SAR distribution was optimized for the best ratio of total SAR in the tumour versus total SAR in muscle and fat. In this SAR distribution the volume of the maximal 4th percentile in muscle is determined. This volume is assigned a weight of 10 in the next optimization step.

Table II : Density and thermal properties of materials and patient tissues. The thermal properties of 'agar' are omitted : this material is not used in the thermal simulations. The entry for 'bolus water' refers to the boli attached to the electrodes, as well as the overlay boli.

material/ tissue	density $\rho(\mathrm{kgm^{-3}})$	spec. heat $\mathrm{Cp(Jkg^{-1}K^{-1})}$	therm. cond $\mathrm{k(Wm^{-1}K^{-1})}$	perfusion ml $100\mathrm{gr^{-1}min^{-1}}$
bolus water	1000	4180	6.0	0
water	1000	4180	0.60	0
air	1.3	1000	0.02	0
muscle	1050	3639	0.56	22
fat	888	2387	0.22	6.8
bone	1595	1420	0.65	0.77
tumour	1050	3639	0.56	11
agar	1000	—	—	—

The effect of this step is a reduction of the SAR maxima in muscle.　The 4th percentile is selected because it generates a volume large enough to have effect in the second optimizing step.　In the third step the largest two of the remaining unwanted SAR maxima are manually outlined and assigned an extra weight in the range of 50 to 125, depending on the size of the volume.

SAR distributions can be quantitatively compared using three performance indicators, the tumour index (Ti), muscle maximum index (MMi) and the fat maximum index (FMi) [28], defined as :

$$Ti = \frac{SAR_{50} \text{ (tumour)}}{SAR_{50} \text{ (totalpatient)}} \tag{2}$$

$$MMi = \frac{SAR_1 \text{ (muscle)}}{SAR_{50} \text{ (tumour)}} \tag{3}$$

$$FMi = \frac{SAR_1 \text{ (fat)}}{SAR_{50} \text{ (tumour)}} \tag{4}$$

where SAR_{50} (Q) is the median SAR in the sub volume Q and SAR_1 (Q) is the value indicating the highest percentile of the SAR distribution in the indicated tissue type.　The Tumour index Ti indicates the ability of the applicator to selectively direct energy into the tumour.　The Muscle Maximum index MMi gives the level of the highest percentile of the SAR distribution in muscle with respect to the median value in tumour, i. e. it indicates the level of the maxima in muscle.　The Fat Maximum index FMi is an equivalent ratio for fat.　A good applicator should be able to generate a high Ti and low MMi and FMi.

Thermal model

The temperature distributions have been computed from the power density distributions using the DIVA thermal model [38], without accounting for the effect of the discrete vasculature.　The tissue blood perfusion was modelled by means of a heatsink [39].　The tumour perfusion was taken half the value of the surrounding muscle tissue [23] [40].　The thermal properties of tissue (Table II) have been taken from the ESHO Taskgroup Committee [32].

In the thermal simulations the power density distribution is scaled to a total absorbed power in the patient volume sufficient to obtain a median tumour temperature of approximately 42°C.　In the RF8 simulation the temperature of the bolus bags, the metal electrodes and the overlay boli was kept at a constant value of 0°C [8] [9], ambient air at 22°C.　In the cavity slot simulation the temperature of the tap water bolus is set at a constant value of 34°C.　The temperature at the cranial and caudal cut off planes was kept constant at 37°C in both applicator types.

The simulation time was set at 2000 s with a time step of 0.25s ; the temperature after 8000 time steps is within 0.1°C of stationarity.　Calculation of the temperature distribution takes less then 15 minutes on a 800 MHz standard personal computer and requires about 7.5 MB RAM.

Results

Agar bone phantom

Fig. 2 (a) and 2 (c) show the SAR distribution in the agar-bone phantom generated by a capacitive
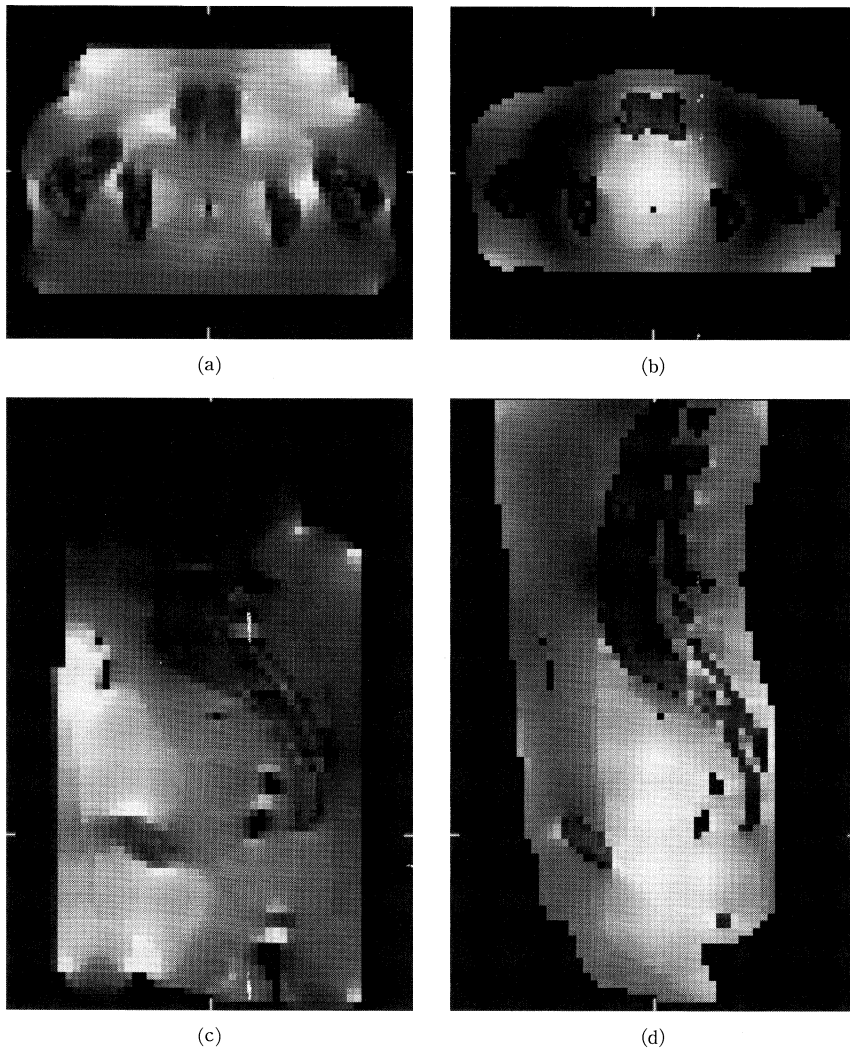
(a)

(b)

(c)

(d)

Fig. 2 : SAR distribution in the patient shaped agar-bone phantom, generated in (a), (c)
the RF8 applicator and (b), (d) in the CS applicator. (a), (b) transversal and (c),
(d) sagittal slice. The slices are taken centrally through the tumour location.
Black and white indicate SAR values from 0 to 125Wkg^{-1}

heating device operating at 8 MHz, the SAR distribution after three step optimization in the cavity slot
applicator operating at 150 MHz is shown in Fig. 2 (b) and 2 (d). Both sagittal and transversal slices
are taken in the same planes, the slices are taken centrally through the tumour, indicated by the markers
in Fig. 2. The SAR distributions are normalized at a total absorbed power of 700 W in the phantom
volume.

The capacitive SAR distribution is characterized by maxima at the edge of the anterior bolus bag and
in the constrictions between the bone elements in the pelvic region (Fig. 2 (a)). The SAR in the tumor
location is relatively low, due to a shielding effect of the pelvic bone. The radiative SAR distribution
shows a distinct maximum in the tumor location and minor submaxima anterior to the symphysis os
pubica and in the lumbo sacral region. These submaxima were partly suppressed in the three step
optimization process. Comparison of the SAR distribution along an anterior-posterior track (dashed

line in Fig. 1 (c)) centrally through the tumour (Fig. 3) shows that the SAR in the tumour is exceeded by anterior and posterior peaks in the RF8 applicator. The SAR track in the cavity slot applicator, on the other hand, shows a threefold increase in SAR in the tumour for the same total absorbed power in the patient and an ample reduction of the anterior and posterior peaks with respect to the tumour. This is also expressed in the performance indices (Table III).
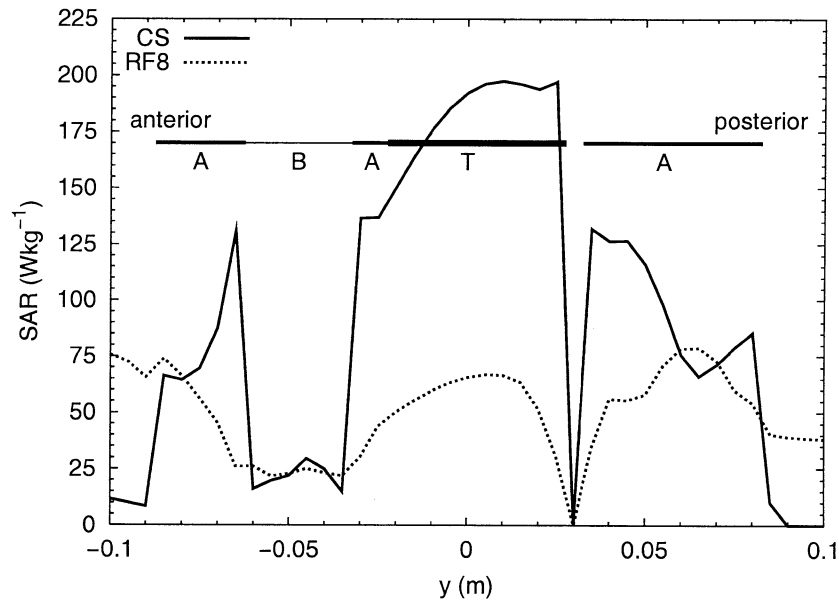

Fig. 3: SAR profiles, anterior-posterior centrally in the tumour location in the patient shaped agar-bone phantom. Both SAR distributions normalized at 700 W total absorbed power.

Table III: SAR performance indices in agar-bone phantom, comparison of RF8 and cavity slot (CS) applicator.

tissue	index	RF8	CS
tumour	Ti	2.5	5.6
agar	AMi	2.7	0.87

SAR in patient model

Fig. 4 (a) and 4 (c) show the SAR distribution in the patient model generated by the RF8 applicator. The SAR distribution after three step optimization in the cavity slot applicator is shown in Fig. 4 (b) and 4 (d). Both sagittal and transversal slices are taken centrally in the tumour. To allow comparison, both SAR distributions are normalized at an equal total absorbed power in the patient volume (700 W).

Comparison of Fig. 2 (a) and 4 (a) shows the influence of the subcutaneous fat layer on the capacitive SAR distribution. Due to the perpendicular orientation of the $\vec{E}$-field on the fat-muscle boundary the SAR in fat is very high with respect to the adjacent muscle [41]. A distinct SAR maximum occurs below the lower part of the anterior electrode (Fig. 4 (a)) due to the redistribution of current to the location where muscle is in direct contact with the bolus bag.

The radiative SAR distribution in the patient model is characterized by a very low absorption in fat (Fig. 4 (b). Some SAR maxima occur in the lumbo-sacral region, the perineum and round the omphalos

(navel) (Fig. 4 (d)).   These unwanted maxima could not fully be eliminated by increasing the weight of these subvolumina in the objective function without creating new SAR maxima.   However, the main SAR maximum is located in the tumour volume.

For a quantitative comparison of the SAR distribution in both applicators, the performance indices are tabulated in Table IV.   The improved SAR concentration in the tumour is expressed by a twofold increase of the tumour index (Ti) in the cavity slot applicator with respect to the RF8 applicator.   The reduction of both muscle and fat maximum indices indicate the improvement of the SAR distribution outside the tumour volume.
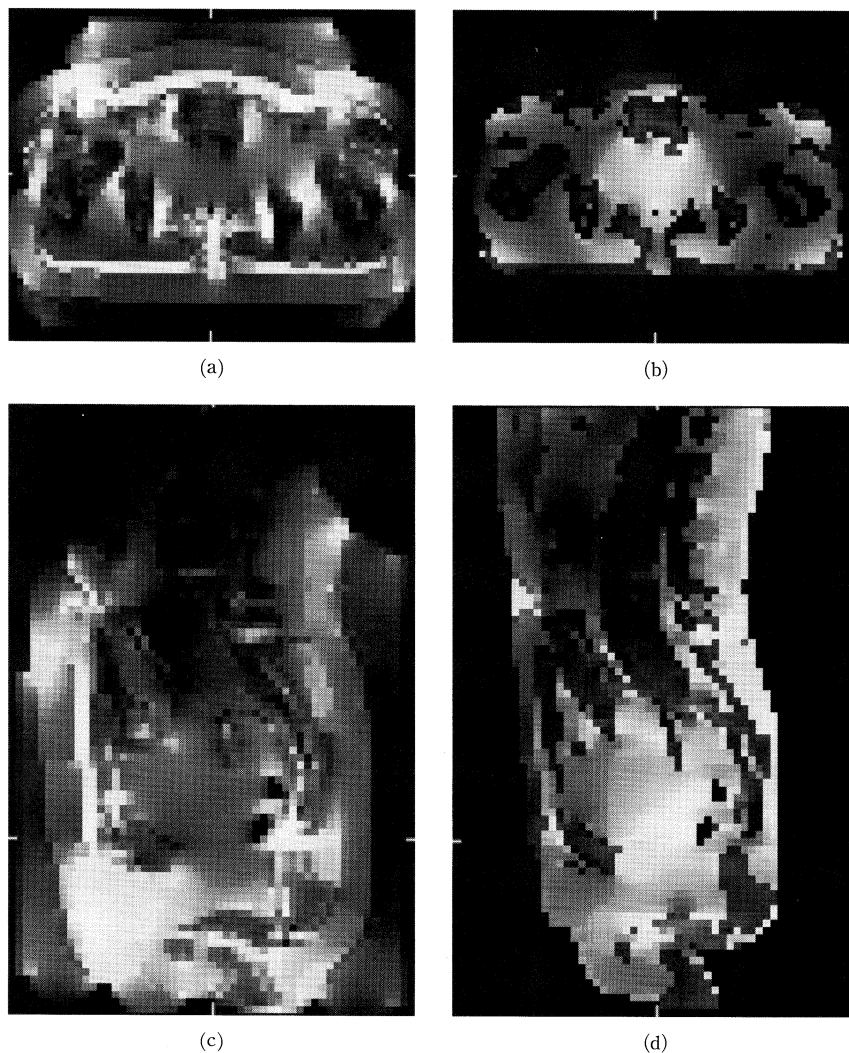

(a)

(b)

(c)

(d)

Fig. 4 : SAR distribution in the patient volume generated in (a, c) the RF8 applicator with
overlay boli and (b, d) in the cavity slot applicator, (a, b) transversal and (c, d)
sagittal Slice.   The slices are taken centrally through the tumour.   Black and white
indicate SAR values from 0 to 125Wkg^{-1}

Fig. 5 shows SAR profiles along the anterior-posterior track (dashed line in Fig. 1 (c)).   The anterior SAR peak in the RF8 applicator is located in the fat layer, the posterior SAR peak is located in a narrow muscle conduit wedged between two fat volumes.   The SAR track in the cavity slot

applicator is more smooth, with an almost constant SAR value in the tumour and moderate peaks in the anterior and posterior muscle volume.
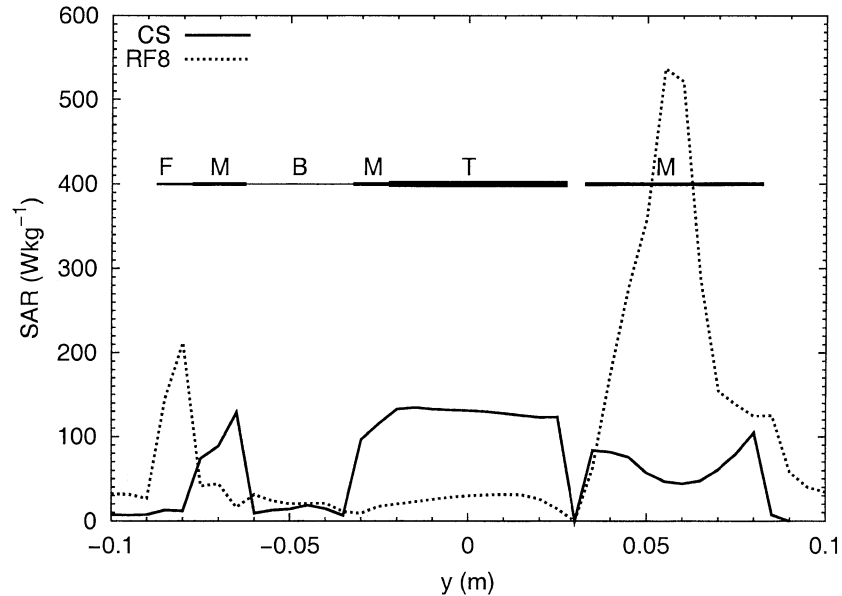

Fig. 5 : SAR profiles, anterior-posterior centrally in the tumour location in the patient model.
　　　　Comparison of cavity slot (CS) applicator and RF8 applicator with overlay boli.
　　　　Both SAR distributions normalized at 700 W total absorbed power.

Temperature

The total power in the patient volume has been scaled to a value sufficient to reach a median tumour temperature of 42°C. The required total absorbed power in the patient in the RF8 applicator is 800 W, in the cavity slot applicator 270 W.

Fig. 6 shows the simulated temperature distributions for both applicators. Fig. 6 (a) and 6 (c) show maxima in the anterior and posterior regions adjacent to the electrodes (Fig. 6 (c)) of the RF8 applicator. However, the SAR maximum in the thin (1 cm) posterior fat layer did not cause a temperature maximum at the same location (Fig. 6 (a)). Apparently the cooling effect of the posterior overlay bolus is sufficient to suppress this unwanted maximum. The bolus cooling effect is, however, not able to completely reduce the anterior maximum, there remain regions with a temperature exceeding 46°C. The thickness of the anterior fat layer locally exceeds 1.5 cm, which is considered the limit for effective skin cooling [2] [42]. The cavity slot applicator (Fig. 6 (b) and 6 (d)) generates a temperature maximum in the tumour volume and minor submaxima in the lumbo-sacral region and round the omphalos. There is no excessive heating of fat layers.

For quantitative comparison of the temperature distributions a cumulative histogram is given in Fig. 7. The temperature curves in the tumour are almost equal, due to scaling of the total absorbed power in the patient volume. However, the temperature distribution in muscle and fat in the RF8 extends to very high values with a T_{10} (muscle) = 43.0°C, T_1 (muscle) = 46.6°C and T_{10} (fat) = 43.5°C, T_1 (fat) = 48. 7°C. The temperature elevation in muscle and fat in the cavity slot applicator is moderate with T_{10} (muscle) = 39.3°C, T_1 (muscle) = 41.1°C and T_{10} (fat) = 38.9°C, T_1 (fat) = 40.2°C. For easy comparison
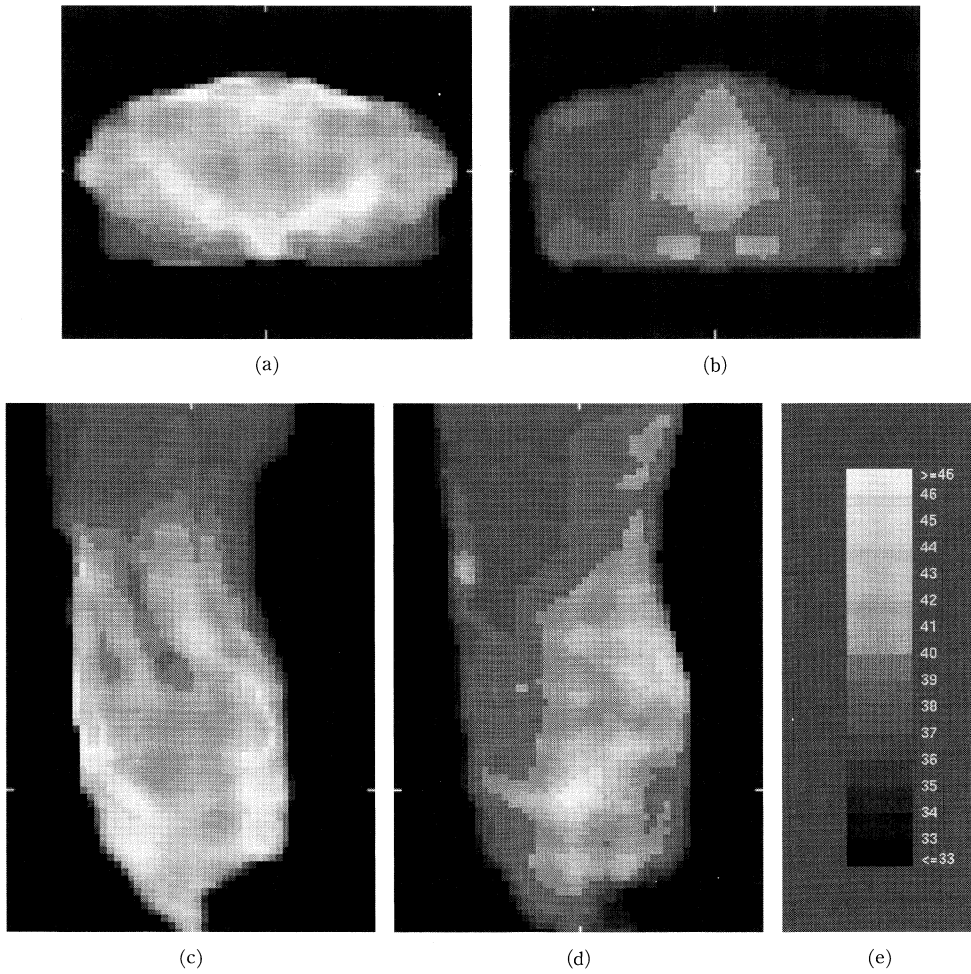
(a)

(b)

(c)

(d)

(e)

Fig. 6 : Temperature distribution in the patient volume generated in (a, c) the RF8 applicator and (b, d) in the cavity slot applicator. (a, b) Transversal and (c, d) sagittal slice. The slices are taken centrally through the tumour. (e) Temperature scale, for clarity the temperatures are truncated to 15 discrete levels from 32°C to 47°C.
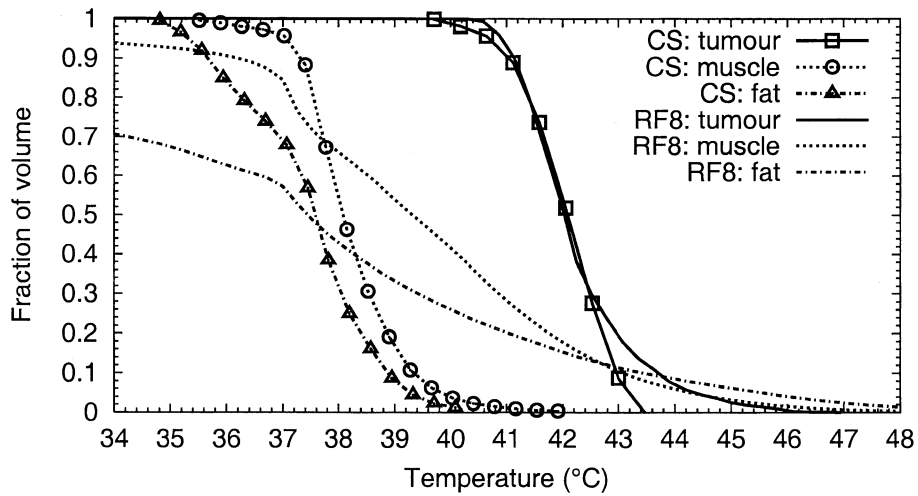

Fig. 7 : Cumulative histogram of the temperature distribution in the patient.

Table IV : Performance indices, comparison of RF8 and cavity slot applicator.

base	tissue	index	RF8	CS
SAR	tumour	Ti	2.2	4.5
	muscle	MMi	2.3	1.6
	fat	FMi	5.2	0.7
temperature	tumour	T_{90}	41.1	41.1
		T_{50}	42.0	42.1
		T_{10}	43.7	43.3
	muscle	T_{10}	43.0	39.3
		T_1	46.6	41.1
	fat	T_{10}	43.5	38.9
		T_1	48.7	40.2

the temperature indices are tabulated in Table IV.

Discussion

In a patient the SAR distribution during regional hyperthermia treatment largely depends on the patient anatomy and the $\vec{E}$-field orientation of the applicator. As shown in the agar-bone phantom the configuration of the pelvic bone prevents optimal heating of a central tumour in a capacitive applicator. The isolating bone deflects the RF-current away from the centre, resulting in SAR maxima outside the tumour volume. The performance of the radiative applicators, however, is only partly influenced by the bone structure. The applicator is able to produce a distinct SAR maximum in the tumour volume.

A realistic patient anatomy, including fat layers, however, disturbs the SAR pattern in both applicator types. The orientation of the $\vec{E}$-field in a capacitive applicator is mainly perpendicular to the fat-muscle boundary, causing high SAR values in the fat layer despite the low conductivity of fat. The application of saline overlay bolus techniques [7-9], body earthing techniques [43] and impedance matching, or subtrap methods [44] can be employed to circumvent this. However, comparison of the RF8 SAR track in the agar-bone phantom (Fig. 3) and in the patient model (Fig. 5) shows that even the relatively thin fat layers of this patient model cause a significant reduction of the SAR value in the tumour and an increase of the anterior and posterior SAR peaks, despite optimization using overlay boli.

The good SAR distribution obtained in the cavity slot applicator demonstrates the favourable properties of multi-ring radiative annular phased array applicators [23] [24] [28]. The $\vec{E}$-field orientation in the central transversal plane in a radiative applicator is oriented parallel to the fat-muscle boundary, resulting in very low SAR values in the superficial fat layer. However, outside the central transversal plane the $\vec{E}$-field is not everywhere oriented perfectly, causing unwanted maxima in the lumbo-sacral region, the perineum and near the omphalos. The optimization process is only partly able to suppress these maxima. Comparison of the cavity slot SAR track in the agar-bone phantom (Fig. 3) and in the patient model (Fig. 5) show also a reduction of the SAR value in the tumour caused by the fat structure, however, the ratio with the anterior and posterior peaks remains fair.

The marked difference in the SAR distributions in both applicator types naturally lead to different temperature distributions. The low SAR values in the tumour generated by the capacitive applicator lead to a high total absorbed power to obtain a median tumour temperature of 42°C. The high superficial SAR values cause temperature maxima outside the tumour volume that will probably cause

sweating, thermoesthesia and fatigue, and limit the RF power[42]. The SAR maximum in the tumour generated by the radiative applicator allows a significant reduction of the total absorbed power needed to attain the tumour target temperature. This will reduce systemic stress and general discomfort. The unwanted SAR maxima outside the tumour volume cause only minor temperature maxima. The superficial temperature can be maintained low with minor skin cooling.

It has to be noticed, however, that the results obtained with the radiative applicator are theoretical and depend on the ability to optimize and control the SAR distribution. This implies full phase amplitude control of the system and accurate similarity of the patient position and posture in the applicator with the patient model used in the treatment planning process. We recently showed that a mere displacement of 2 cm of the patient already causes a deterioration of the performance indices[28]. Seebass *et al.*[27] investigated the influence of amplitude and phase errors at frequencies from 100 MHz to 200 MHz on the temperature distribution and found that this influence decreased with the increase of frequency.

Conclusion

New phase amplitude controlled radiative regional hyperthermia is a good alternative for capacitive techniques in the treatment of tumours in the pelvic region.

The radiative coupling of the patient to the applicator avoids by nature some of the known disadvantages of capacitive systems, such as high superficial heating and thermoesthesia. The large number of degrees of freedom enables the optimizing process to reduce treatment limiting SAR maxima. Whether these promising theoretical results can be obtained in daily clinical practice depends on progress in the field of phase amplitude control, applicator design and high-resolution hyperthermia treatment planning.

References

1) Tanaka H., Kato H., Nishida T., Kano E., Sugahara T., Ishida T. : Physical basis of RF hyperthermia for cancer therapy (2) Measurement of distribution of absorbed power from radio frequency exposure in agar phantom. Journal of Radiation Research, 22 : 101-108, 1981.

2) Kato H., Hiraoka M., Nakajima T., Ishada T.. Deep-heating characteristics of an RF capacitive heating device. International Journal of Hyperthermia, 1 : 15-28, 1985.

3) Harima Y., Nagata K., Harima K., Atsutoshi O., Ostapenko V. V., Shikata N., Ohnishi T., Tanaka Y.. Bax and Bcl-2 protein expression following radiation therapy versus radiation plus thermoradiotherapy in stage IIIb cervical carcinoma. Cancer, 88 : 132-138, 2000.

4) Kroeze H., Van de Kamer J. B., De Leeuw A. A. C., Kikuchi M., Lagendijk J. J. W.. Treatment planning for capacitive regional hyperthermia. International Journal of Hyperthermia, (accepted) 2002.

5) Hiraoka M., Jo S., Akuta K., Y. N., Takahashi M., Abe M.. Radiofrequency capacitive hyperthermia for deep-seated tumours. Cancer, 60 : 121-127, 1987.

6) Rhee J. G., Lee C. K. K., Osborn J., Levitt S. H., Song C. W.. Precooling prevents overheating of subcutaneous fat in the use of RF Capacitive heating. International Journal of Radiation Oncology, Biology and Physics, 20 : 1009-1015, 1991.

7) Kato H., Hyodo K., Akassa N., Nishimura K., Uchida N., Kasai T., Sugimura K.. Optimization of bolus for

capacitive type heating.　Japanese Journal of Hyperthermic Oncology, 13 : 10-17. (Japanese) 1997.

8) Tomimatsu A., Imada H., Kosaka K., Nomoto S., Kusano S., Ostapenko V. V., Terashima H.. Advantage of an external cooling unit in deep hyperthermia using an 8 MHz RF capacitive heating device. Japanese Journal of Hyperthermic Oncology, 15 : 65-70, 1999.

9) Tomimatsu A., Imada H, Kosaka K, Nomoto S., Kusano S., Ostapenko V. V., Terashima H.　Refinement of circulating liquid of overlay bolus in hyperthermia using an 8 MHz RF capacitive heating device. Japanese Journal of Hyperthermic Oncology, 15 : 71-77, 1999.

10) Lee C. K., Song C. W., Rhee J. G., Foy J. A., Levitt S. H.. Clinical experience using 8 MHz Radiofrequency capacitive hyperthermia in combination with radiotherapy : results of a phase I/II study.　International Journal of Radiation Oncology, Biology and Physics, 32 : 733-745, 1995.

11) Turner P. F.. Regional hyperthermia with an annular phased array.　IEEE Ttansactions on Biomedical Engineering, 31 : 106-114, 1984.

12) Turner P. F., Schaeffermeyer T.. BSD-2000 approach for deep local and regional hyperthermia.　Strahlentherapie und Onkologie, 165 : 738-741, 1989.

13) Van Dijk J. D. P., Gonzalez-Gonzalez D., Blank L. E. C. M.. Deep local hyperthermia with a four aperture array system of large waveguide radiators.　Results of simulation and clinical application.　In Sugahara T., Saito M., eds., Hyperthermic Oncology 1988, volume 1 Summary Papers.　London, UK : Taylor & Francis, 573-575, 1989.

14) De Leeuw A. A. C., Lagendijk J. J. W.. Design of a deep-body hyperthermia system based on the 'Coaxial TEM' applicator.　International Journal of Hyperthermia, 3 : 413-421, 1987.

15) Van der Zee J., Gonzalez Gonzalez D., Van Rhoon G. C., Van Dijk J. D. P., Van Putten W. L. I., Hart A. A. M.. Comparison of radiotherapy alone with radiotherapy plus hyperthermia in locally advanced pelvic tumours : a prospective, randomised, multicentre trial.　The Lancet, 355 : 1119-1125, 2000.

16) Dinges S., Harder C., Wurm R., Buchali A., Blohmer J., Gellermann J., Wust P., Randow H., Budach V.. Combined treatment of inporable carcinomas of the uterine cervix with radiotherapy and regional hyperthermia.　Strahlentherapie und Onkologie, 174 : 517-521, 1998.

17) Van Vulpen M., De Leeuw A. A. C., Van de Kamer J. B., Kroeze H., Boon T. A., Warlam-Rodenhuis C. C., Lagendijk J. J. W., Battermann J. J.. Regional Hyperthermia combined with radiotherapy for locally advanced prostate carcinoma, a feasibility study with special attention to the use of invasive thermometry.　International Journal of Hyperthermia 2002 ; (submitted).

18) Van Es C. A., Wijrdeman H. K., De Leeuw A. A. C., Mooibroek J., Lagendijk J. J. W., Battermann J. J.. Regional hyperthermia of pelvic tumours using the Utrecht Coaxial TEM system : a feasibility study.　International Journal of Hyperthermia, 11 : 173-186, 1995.

19) Rau B., Wust P., Hohenberger P., Loffel J., Hunerbein M., Below C., Gellermann J., Speidel A., Vogl T., Riess H., Felix R., Schlag P. M.. Preoperative hyperthermia combined with radiochemotherpay in locally advanced rectal cancer.　Annals of Surgery, 227 : 380-389, 1998.

20) Egawa S., Tsukiyama I., Akine Y., Kajiura Y., Ogino T., Yamashita K.. Hyperthermic therapy of deep seated tumors : comparison of the heating efficiencies of an annular array applicator and a capacitively coupled radiofrequency system.　International Journal of Radiation Oncology, Biology and Physics, 14 : 512-528, 1988.

21) Sullivan D. M.. Mathematical methods for treatment planning in deep regional hyperthermia.　IEEE Transactions on Microwave Theory and Technique, 39 : 864-872, 1991.

22) Clegg S. T., Das S. K., Fullar E., Anderson S., Blivin J., Oleson J. R., Samulski T. V.. Hyperthermia treatment planning and temperature distribution recon struction : a case study.　International Journal of Hyperthermia, 12 : 65-76, 1996.

23) Wust P., Seebass M., Nadobny J., Deuflhard P., G. M., Felix R.. Simulation studies promote technological develop-

ment of radiofrequency phased array hyperthermia. International Journal of Hyperthermia, 12 : 477-494, 1996.

24) Paulsen K. D., Geimer S., Tang J., Boyse W. E.. Optimization of pelvic heating rate distributions with electromagnetic phased arrays. International Journal of Hyperthermia, 15 : 157-186, 1999.

25) Van de Kamer J. B., De Leeuw A. A. C., Hornsleth S. N., Kroeze H, Kotte A. N. T. J., Lagendijk J. J. W.. Development of a regional hyperthermia treatment planning system. International Journal of Hyperthermia, 17 : 207-220, 2001.

26) Van de Kamer J. B., Van Vulpen M., De Leeuw A. A. C., Kroeze H., Lagendijk J. J. W.. CT-resolution regional hyperthermia treatment planning. International Journal of Hyperthermia, 18 : 104-116, 2002.

27) Seebass M., Beck R., Gellermann J., Nadobny J., Wust P.. Electromagnetic phased arrays for regional hyperthermia : optimal frequency and antenna arrangement. International Journal of Hyperthermia, 17 : 321-36, 2001.

28) Kroeze H., Van de Kamer J. B., De Leeuw A. A. C., Lagendijk J. J. W.. Regional hyperthermia applicator design using FDTD modelling. Physics in Medicine and Biology, 46 : 1919-1935, 2001.

29) Hornsleth S. N., Mella O., Dahl O.. A new CT segmentation algorithm for finite difference based treatment planning systems. In Ftanconi C., Arcangeli G., Cavaliere R., eds., Hyperthermic Oncology 1996, volume 2. Rome, Italy : Tor Vergata, 521-523, 1996.

30) James B. J., Sullivan D. M.. Creation of three-dimensional patient models for hyperthermia treatment planning. IEEE Transactions on Biomedical Engineering, 39 : 238-242, 1992.

31) Stogryn A.. Equations for calculating the dielectric constant of saline water. IEEE Transactions on Microwave Theory and Technique, 19 : 733-736, 1971.

32) ESHO Taskgroup Committee. Treatment Planning and Modelling in Hyperthermia, a Task Group Report of the European Society for Hyperthermic Oncology. Rome, Italy : Tor Vergata 1992.

33) Gabriel C., Gabriel S., Corthout E.. The dielectric properties of biological tissues : I. literature survey. Physics in Medicine and Biology, 41 : 2231-2249, 1996.

34) Van de Kamer J. B., Van Wieringen N., De Leeuw A. A. C., Lagendijk J. J. W.. The significance of accurate dielectric tissue data for hyperthermia treatment planning. International Journal of Hyperthermia, 17 : 123-142, 2001.

35) De Bree J.. A 3-D anatomy based treatment planning system for interstitial hyperthermia. Ph. D. thesis, Utrecht University 1998.

36) Piket-May M., Taflove A., Baron J.. FD-TD modeling of digital signal propagation in 3-D circuits with passive and active loads. IEBE Transactions on Microwave Theory and Technique, 42 : 1514-1523, 1994.

37) Sullivan D. M., Ben-Yosef R., Kapp D. S.. Stanford 3D hyperthermia treatment planning system. Technical review and clinical summary. International Journal of Hyperthermia, 9 : 627-643, 1993.

38) Kotte A. N. T. J., Van Leeuwen G. M. J., De Bree J., Van der Koijk J. F., Crezee J., Lagendijk J. J. W.. A description of discrete vessel segments in thermal modelling of tissues. Physics in Medicine and Biology, 41 : 865-884, 1996.

39) Pennes H. H.. Analysis of tissue and arterial blood temperature in the resting human forearm. Journal of Applied Physiology, 1 : 93-122, 1948.

40) Van Vtlpen M., Raaymakers B. W., De Leeuw A. A. C., Van de Kamer J. B., van Moorselaar R. J. A., Hobbelink M. G. G., Battermann J. J., Lagendijk J. J. W.. Prostate perfusion in patients with locally advanced prostate carcinoma, measured during different hyperthermia techniques. Journal of Urology 2002 ; (accepted).

41) Lagendijk J. J. W., De Leeuw A. A. C.. The development of applicators for deep body hyperthermia. In Recent Results in Cancer Reserach. Springer Verlag, 18-35, 1986.

42) Nomoto S., Imada H., Tomimatsu A., Kosaka K., Kusano. S., Ostapenko V. V., Terashima H.. Side effects of Hyperthermia for intrathorac tumors using an 8 MHz RF capacitive heating device. Japanese Journal of Hyperthermic Oncology, 15 : 9-14, 1999.

43) Kosaka K., Imada H., Tomimatsu A., Nomoto S., Kusano. S., Ostapenko V. V., Terashima H.. Effectiveness of body

earthing in hyperthermia using an 8 MHz RF capacitive heating device. Japanese Journal of Hyperthermic Oncology, 15: 1-7, 1999.

44) Murata T., Akagi K., Ostapenko V. V., Isoda H., Nagata K., Nasu R., Shiga T., Tanaka Y., Yamamoto I.. Relevance of a new impedance matching, or subtrap method for the reduction of pain during hyperthermia.　Acta Oncologica, 37: 485-488, 1998.

領域加温における誘電型加温法と放射型加温法との比較

Hugo Kroeze[1]・小久保雅樹[2]・Jeroen B. Van de Kamer[1]・Astrid A. C. De Leeuw[1]
菊 地　　眞[3]・平 岡 眞 寛[4]・Jan J. W. Langendijk[1]

[1]ユトレヒト大学メディカルセンター放射線腫瘍学
[2]先端医療センター映像医療研究部
[3]防衛医科大学校医用電子工学
[4]京都大学医学研究科腫瘍放射線科学

要　　旨：領域加温における誘電型加温法と放射型加温法を，ファントムモデルと前立腺患者をモデルとして用いて比較した．誘電型加温のモデルには，8MHz 装置 (サーモトロン RF8) を用いた．この加温性能は適切な塩分濃度で極低温にしたオーバーレイボーラスを使用することで改善した．放射型加温には3列のリングアレイ型アンテナを用い，150MHz の電流を給電した．放射型においては，位相，振幅を制御することにより，単位質量あたりのエネルギー吸収率 (SAR) を最適化した．SAR と温度分布を比較したところ，放射型加温では骨盤内腫瘍に関して良好な温度分布が得られ，誘電型加温で見られたような皮下脂肪，筋組織でのホットスポットを防ぐことができた．